Reduction of the bulk modulus at high pressure in CrN

Francisco Rivadulla[1]*, Manuel Bañobre-López[1], Camilo X. Quintela[2], Alberto Piñeiro[2,3], Victor Pardo[2,3], Daniel Baldomir[2,3], Manuel Arturo López-Quintela[1], José Rivas[2], Carlos A. Ramos[4], Horacio Salva[4], Jian-Shi Zhou[5] and John B. Goodenough[5]

Nitride coatings are increasingly demanded in the cutting- and machining-tool industry owing to their hardness, thermal stability and resistance to corrosion. These properties derive from strongly covalent bonds; understanding the bonding is a requirement for the design of superhard materials with improved capabilities. Here, we report a pressure-induced cubic-to-orthorhombic transition at ≈1 GPa in CrN. High-pressure X-ray diffraction and *ab initio* calculations show an unexpected reduction of the bulk modulus, K_0, of about 25% in the high-pressure (lower volume) phase. Our combined theoretical and experimental approach shows that this effect is the result of a large exchange striction due to the approach of the localized Cr:t^3 electrons to becoming molecular-orbital electrons in Cr–Cr bonds. The softening of CrN under pressure is a manifestation of a strong competition between different types of chemical bond that are found at a crossover from a localized to a molecular-orbital electronic transition.

The four sp^3 hybrids of carbon in diamond form the strongly covalent and directional bonds responsible for its hardness and ultralow compressibility. These properties make diamond widely used in coatings, polishing and cutting in the tool industry even though the cost of its artificial synthesis and its ineffective cutting of ferrous materials limit its practical applications. Group IV nitrides, BN, PtN and some metallic carbides or borides present a set of mechanical properties that could make these materials an alternative to diamond[1–4]. However, some of them are economically and environmentally expensive as a result of synthesis under extreme conditions, which has hampered their widespread application. On the other hand, chromium nitride (CrN) has raised many expectations over recent years as it combines an ease of film deposition, high thermal stability and corrosion resistance with the prediction of a very large bulk modulus ($K_0 \approx 361$ GPa; refs 5, 6). Yet, in spite of this high potential, experimental measurements of K_0 in CrN are lacking. This lack of data is most probably due to the difficulty of preparing stoichiometric samples, which has resulted in different and even contradictory reports about its structural and electrical properties[7,8].

Here we report a drastic, about 25%, reduction of K_0 in stoichiometric CrN above ≈1 GPa. Combining the experimental structural and magnetic data with *ab initio* calculations, we demonstrate that this anomalous softening has its origin in a purely electronic effect.

The results of the X-ray diffraction experiments at different temperatures and pressures are summarized in Fig. 1. All the results discussed in this work correspond to polycrystalline samples synthesized by ammonolysis of Cr_3S_4. We have developed this method, which presents many advantages over similar synthetic routes that use Cr_2S_3 as a starting material (see Methods section). Previous studies[9,10] showed that stoichiometric CrN presents a cubic rock-salt (space group *Fm3m*) paramagnetic structure at high temperature that becomes orthorhombic (space group *Pnma*) and antiferromagnetic (AF) below 285 K; the structural transition was tentatively attributed to a large exchange-striction effect[11]. We observed the first-order structural transition at 286±1 K (282±1 K) with increasing (decreasing) temperature (inset to Fig. 1 and Supplementary Fig. S1). The volume change at the transition is 0.56%, as determined from the Rietveld fitting of the X-ray patterns at different temperatures. Comparing the structural data with the systematic study in ref. 10 corroborates that our samples are of the highest quality (see Supplementary Information for details).

The pressure dependence of the volume was measured up to 20 GPa with synchrotron radiation (Fig. 1). At room temperature we observed a pressure-induced structural transition at ≈1 GPa from the low-pressure *Fm3m* to the high-pressure *Pnma* structure. The small dependence of the peak positions on pressure, particularly below 1 GPa, indicates a very small compressibility that increases somewhat at higher pressures. The lattice parameters under pressure were refined by Rietveld fitting of the X-ray patterns, and the volume–pressure data were fitted to the Birch–Murnaghan equation[12]

$$P = 3K_0 f_E (1+2f_E)^{5/2}\left(1+\frac{3}{2}(K'-4)f_E\right) \qquad (1)$$

where K_0 is the zero-pressure bulk modulus, $K' = \partial K_0/\partial P$ and $f_E = 1/2[(V_0/V)^{2/3}-1]$ is the Eulerian strain. The results are shown in Fig. 2 with K' fixed to the canonical value of four.

We have observed ≈1% difference between the lattice parameters determined at ambient pressure inside the diamond anvil cell and those obtained in the conventional X-ray laboratory set-up used for the temperature scans. For this reason, the zero-pressure volume V_0 used in this plot was determined in the same experimental

[1]Physical-Chemistry Department, University of Santiago de Compostela, 15782-Santiago de Compostela, Spain, [2]Applied Physics Department, University of Santiago de Compostela, 15782-Santiago de Compostela, Spain, [3]Instituto de Investigaciones Tecnológicas, Universidad de Santiago de Compostela, E-15782, Santiago de Compostela, Spain, [4]Centro Atómico de Bariloche, 8400 San Carlos de Bariloche, Rio Negro, Argentina, [5]Texas Materials Institute, ETC 9.102, The University of Texas at Austin, Austin, Texas 78712, USA. *e-mail: f.rivadulla@usc.es.

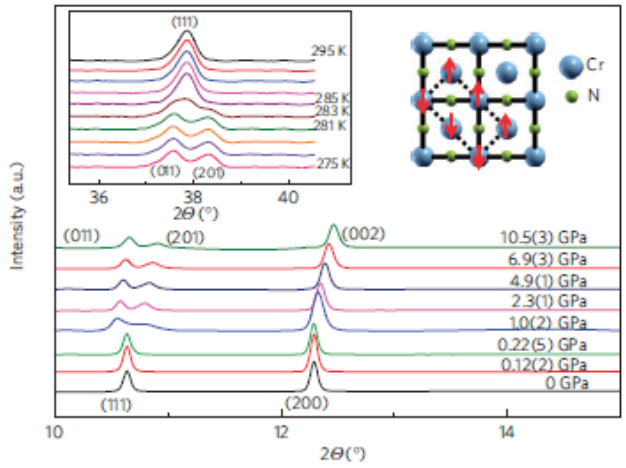

Figure 1 | Summary of the X-ray results at different pressures and temperatures. The peaks occur at different angles, 2Θ, in the temperature and pressure runs owing to the different wavelengths used for the two experiments (see Methods section). At room temperature, the transition between the low-pressure *Fm3m* and high-pressure *Pnma* phase occurs at ≈1 GPa with increasing pressure. Left inset: Detail of the evolution of the X-ray pattern taken with decreasing temperature across the *Fm3m*-to-*Pnma* transition. Right inset: (001) cation planes of the *Fm3m* structure of CrN, with the *Pnma* unit cell indicated with dashed lines and Cr magnetic order after ref. 9.

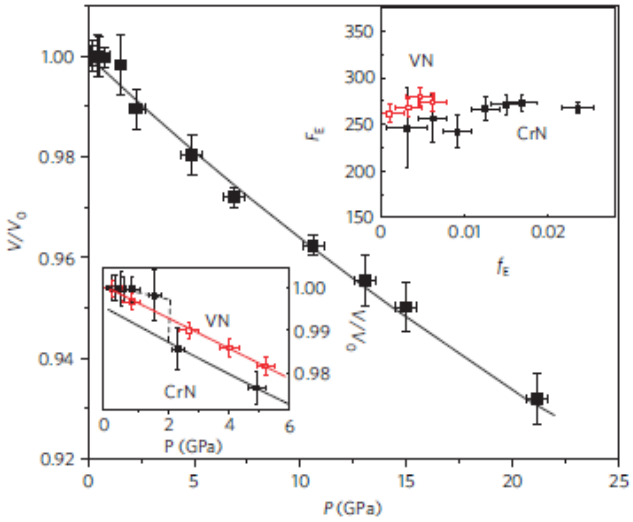

Figure 2 | Volume–pressure data of CrN fitted to the Birch–Murnaghan equation of state, truncated at second order ($K' = 4$). Upper inset: Normalized pressure versus Eulerian strain for the high-pressure orthorhombic phase of CrN and for VN. Lower inset: Comparison of the low-pressure data in CrN and VN. The compressibility of the orthorhombic high-pressure phase in CrN is similar to that of metallic VN and is much smaller than that of cubic CrN. Dashed and solid lines are guides to the eye and fits to the Birch–Murnaghan equation, respectively. Horizontal (vertical) error bars come from the uncertainty in the determination of the pressure (lattice parameters).

conditions as the high-pressure data to minimize the errors. There is a clear break in $V(P)$ at the *Fm3m–Pnma* structural transition with an increase of slope at high pressure (see the lower inset to Fig. 2), which points towards a large reduction in K_0 above the transition. The fittings of $V(P)$ above the structural transition result in $K_0 = 243(10)$ GPa for the orthorhombic structure stable at high pressure. Small variations from $K' = 4$ do not improve the fitting or significantly vary the results. The results at high pressure have been verified through the use of reduced variables, where the reduced pressure is defined as[12]

$$F_E = \frac{1}{3f_E(1+2f_E)^{5/2}}$$

The results are shown in the upper inset to Fig. 2, giving $K_0 = 260(10)$ GPa, similar to the value derived from direct fitting to equation (1).

On the other hand, the small number of points that we were able to place below 1 GPa makes estimation of a reliable value for K_0 in the cubic phase difficult. Also, because of the proper definition of F_E, the error increases very much as P is reduced, making impossible this analysis for the low-pressure cubic phase to double check the large value of K_0 obtained by direct fitting to equation (1).

The change in K_0 is supported by the temperature dependence of the dynamic Young's modulus, E. There is a hardening of the material as well as a strong reduction in the temperature dependence of E of about 40% at the cubic phase with respect to the lower-temperature orthorhombic structure (Supplementary Fig. S3). A strong change was also observed in the internal friction (Supplementary Fig. S3). These experimental results suggest a change in the bulk modulus at the structural phase transition, although we cannot obtain an absolute value for each phase from this experiment.

Previous reports showed E to be in the range of 324–400 GPa (ref. 13), and the Vickers hardness to be 1750 (ref. 14). However, all of them correspond to the phase stable at room temperature, the cubic phase.

Therefore, to provide further confirmation of the reduction of K_0 at the structural transition, as well as to confirm the values measured, we have calculated *ab initio* the bulk modulus in both phases. Our calculations were made with the generalized gradient approximation and the WIEN2k package, on the basis of the full-potential (linearized) augmented plane-wave ((L)APW) + local orbitals (lo) method. We have used the data obtained from the high-resolution synchrotron experiments as the starting point for the structural relaxation. Our calculations show a change from $K_0(Fm3m) = 340(10)$ GPa to $K_0(Pnma) = 255(5)$ GPa, confirming a drastic reduction (≈25%) of the compressibility in the orthorhombic phase.

We have also calculated the values of K_0 within the LDA approximation to the exchange–correlation potential with the WIEN2k code, obtaining the results of 430 GPa for cubic CrN and 260 GPa for orthorhombic CrN. Although the value for the cubic phase is larger in this case, they give strong support to our conclusions about the change in the bulk modulus of CrN at the pressure-induced structural transition. Also, we have calculated a value of 280(10) GPa for VN in the generalized gradient approximation, and 250 GPa within the LDA. Any of them correlates very well (within 10%) with our experimental estimation of 265(5). This agreement provides extra support for the accuracy of our calculations.

The value of the cubic K_0 is among the largest reported in nitrides, comparable to those of PtN_2, IrN_2, MoN, BN, RuN_2 or other systems such as OsB_2 (refs 4, 6, 15–19). Moreover, CrN shows the advantage over the other materials of an easy ambient-pressure and non-hazardous synthesis. In the high-pressure orthorhombic phase, K_0 decreases to values typical for other metallic nitrides such as TiN or VN ($K_0 = 265(5)$ GPa from the plot in the inset to Fig. 2; see also Supplementary Fig. S2).

The strong reduction of K_0 will most probably be reflected in a variation of the hardness of CrN owing to the correlation that normally exists between the two effects, and so an experimental

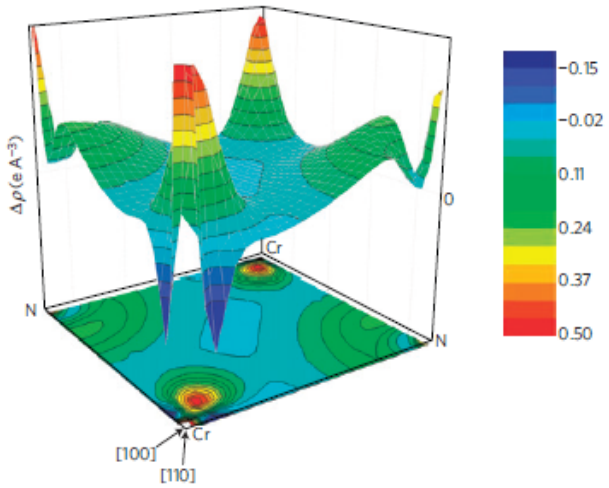

Figure 3 | *Ab initio* calculation of the charge-density difference between the high-pressure *Pnma* and low-pressure *Fm3m* phases of CrN. Cr–Cr and Cr–N distances at both pressures were normalized for the subtraction of electron densities. There is an appreciable charge transfer from the Cr e_g orbitals directed along the covalent Cr–N bond (negative peaks along [100] and [010]) towards the ionic t_{2g} orbitals of the Cr–Cr bonds (positive peaks along [110]). Some degree of charge delocalization along Cr–Cr bonds is observed with increasing pressure, as confirmed by magnetic measurements under pressure (see the text).

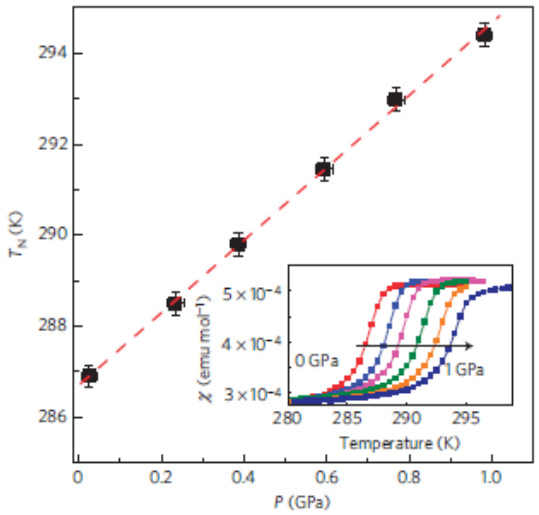

Figure 4 | Pressure dependence of the magnetic transition temperature, T_N, of the *Pnma* phase. The line is a linear fitting to the data. Inset: Temperature dependence of the molar susceptibility at different pressures. The points of the main panel are obtained from the minimum in the derivative of these curves at each pressure.

determination of the hardness in both crystallographic phases is highly desirable. This could have important technological implications, because the *Pnma* phase should be avoided for certain practical applications; note that this transformation will also occur below 285 K at ambient pressure. Similar variations in the hardness/compressibility have been reported in other systems, for example in stressed Zr_3N_4, and BN, to be associated with structural transitions[20,21]. Hence, to design superhard materials with superior capabilities, it is imperative to reach a precise understanding of the changes in the chemical bond that lead to such remarkable effects.

The large K_0 of cubic CrN is presumably due to strong, directional bonds between the Cr:3*d* (e_g) and N:2*p* orbitals that must be modified in the *Pnma* phase at some energy cost. The results of the redistribution of charge density across the structural transition obtained by *ab initio* calculation confirm this point (Fig. 3). There is considerable charge transfer from the Cr orbitals that form the covalent Cr–N bonds towards the Cr–Cr bonds at the transition from the *Fm3m* to the *Pnma* phase. Surprisingly, none of the previous calculations have captured any of these important effects. The increasing instability of the Cr–Cr equilibrium bond length is also manifest in the linear dependence of the lattice thermal conductivity in the cubic phase (Supplementary Fig. S6).

On the other hand, as the *Pnma* phase is stabilized below T_N even at high pressure (Fig. 4), the driving force for the transition must be a strong exchange striction, and the magnetic structure from neutron diffraction[9] should be very helpful to elucidate the nature of the chemical bond in CrN. The magnetic order (Fig. 1, right inset) consists of AF 180° Cr–N–Cr interactions within the (001) planes and ferromagnetic (FM) 180° Cr–N–Cr [001]-axis interactions. As the e_g orbitals of an octahedral-site Cr^{3+} ion are formally empty, only the AF semicovalent exchange component contributes to the 180° Cr–N–Cr interactions[22]. Then, in CrN the magnetic order is driven by a stronger AF Cr–Cr interaction that competes with an FM 90° Cr–N–Cr interaction. Where an FM and an AF interaction of comparable strength compete with each other, as in the (001) planes of $R^{3+}MnO_3$ perovskites, an exchange-density wave consisting of alternating FM and AF interactions may be stabilized[23]. On traversing the [001] and [010] axes, the Cr–Cr interactions alternate between FM and AF as in an exchange-density wave within the (001) and (010) planes. The interactions between the (100) and (010) planes are ordered so as to allow three short Cr–Cr bonds per Cr atom to enhance the AF coupling. A careful inspection of the structural data shows that the ambient-pressure Cr–Cr distance of ~2.933(3)Å in the cubic phase, splits into two non-equivalent distances below the orthorhombic transition: a long one (~2.965(5)Å) along the FM [1$\bar{1}$0] direction, and a short one (~2.883(5)Å) along the AF [110] direction. The Cr–N distance remains practically unchanged. The same effects are observed with increasing pressure, which reduces the short Cr–Cr distance along [110] even more. The charge redistribution associated with this transformation can be seen in Fig. 3. On the other hand, short Cr–Cr bond lengths are close to the itinerant (molecular orbital) electron limit for edge-shared octahedral Cr sites in oxides[22]. At crossover in, for example, $LiVO_2$ and the spinels $Zn[V_2]O_4$, $Cu[Ir_2]S_4$ and $Mg[Ti_2]O_4$, cooperative homopolar bonding is stabilized in M–M pairs at low temperatures[24–26]. Particularly relevant to the present case could be the report of alternate short–long bonds in IrN_2 due to a Peierls distortion[18].

Where the deformation introduced by this cooperative bond formation is resisted by the other bonding in the lattice, as is the case for the strong, directional Cr–N bonds in CrN, the enhanced M–M bonding in the low-temperature phase may only reduce the net localized spin without forming spin-paired homopolar bonds. The thermal hysteresis, the abruptness of the transition and its sensitivity to cation/anion stoichiometry supports the cooperative nature of the transition in CrN. On the other hand, the shape of the $\chi(T)$ curve (see Supplementary Fig. S4) and a low spin moment of 2.5(1) μ_B/Cr decreasing with pressure obtained from our LDA + U calculations are fully compatible with some spin reduction in the AF Cr–Cr bonds.

To test this possibility further, we have monitored the pressure dependence of the magnetic exchange interaction. In a localized-electron system that approaches the localized-to-itinerant electronic crossover, a sharp increase with decreasing Cr–Cr separation in the spin–spin superexchange parameter[27]

$$J \propto \frac{t^2}{U} \qquad (2)$$

occurs because an enhanced screening makes the intra-atomic Coulomb energy U decrease sensitively as the spin-dependent Cr–Cr charge-transfer expectation value t increases. The volume dependence of t has been calculated by Harrison[28] to be $J \propto V^{-10/3}$, which is the basis of the phenomenological Bloch equation[29] for magnetic insulators: $\alpha = (\partial \ln T_N / \partial \ln V) \approx -3.3$. Small deviations from $\alpha = -3.3$ can be used to define the limit of applicability of crystal-field theory on the approach to itinerant-electron behaviour[30]. The results for the pressure dependence of T_N are shown in Fig. 4. The magnetic transition temperature increases at a rate of $d \ln T_N / dP = 2.77 \times 10^{-2}$ GPa^{-1}. As the magnetic phase is the low-temperature *Pnma*, we used $K_0 = 243(10)$ GPa to calculate an $\alpha = -6.7(2)$, much higher than expected from superexchange theory for Cr–Cr superexchange.

This result invalidates the assumption of a pressure-independent energy U in the localized-electron superexchange theory behind equation (2) and confirms a partial electronic delocalization in the *Pnma* phase along the short Cr–Cr bonds. We think that these types of magnetic experiment are very useful in the investigation of the nature of the chemical bond and could be applied to other hard magnetic systems with transition-metal ions[31].

Also, our results suggest that the strong electronic correlations not considered in previous LDA calculations[11] could be an important ingredient to understand the structural instability. It is perhaps pertinent to note that the softer K_0 values of VN and TiN may also be due to an itinerant-electron M–M bond that is longer than its equilibrium value. In these materials, both cation and anion vacancies are introduced to reduce the M–M separation, but at the expense of the M–M bonding. Pressure reduces the M–M separation towards the equilibrium value for itinerant-electron bonding, thereby softening K_0. The Cr–N distances remain practically invariant across the transition, and hence we could assume that their force constant changes little. Then, the higher compressibility of the lower-volume phase is made possible by the longer-than-equilibrium Cr–Cr bond length, which results in a smaller variation of the internal energy with the volume than expected.

In summary, the large K_0 of the cubic phase makes CrN a very incompressible material. However, the material softens dramatically in the low-temperature/high-pressure AF *Pnma* phase. An exchange-striction distortion sensitive to pressure is compatible with a localized t_{2g}^3 configuration on the Cr atoms that approaches the itinerant-electron crossover from the localized-electron side. The approach to crossover commonly results in a cooperative formation of cation clusters in which homopolar or itinerant-electron bonds are formed and electron spins are paired. However, the strong, directional Cr–N bonds apparently resist a deformation that is large enough to pair the spins completely. Softening of the lattice reflects the fact that Cr–Cr bonds between AF-coupled Cr can be strengthened by a pressure that reduces further the Cr–Cr separation against the resistance of directional Cr–N bonds.

These results suggest that the mechanical properties of superhard CrN may be improved through the fabrication of tensioned films or nanostructures that suppress the cooperative cubic-to-orthorhombic transition[8]. The ease of fabrication of nitrides in the form of nanoparticles and sputtered films at mild conditions makes cubic CrN a suitable alternative to other hard systems.

Methods

Synthesis and characterization of the samples. Stoichiometric CrN was synthesized by treating the spinel Cr_3S_4 in an NH_3 flow at 800 °C for 8 h with an intermediate grinding. Cr_3S_4 was previously synthesized in evacuated silica tubes from elemental S and Cr heated at 1,000 °C for 24 h. This method provides pure single-phase samples of CrN with a cubic lattice parameter at room temperature $a = 4.148(1)$Å (see Supplementary Fig. S1), consistent with stoichiometric CrN. This method shows a significant improvement over the results obtained by the ammonolysis of Cr_2S_3 (ref. 7). A similar method was used to prepare VN.

The Cr/N ratio was further verified to be 1.01(2) by X-ray photoemission spectroscopy. The X-ray photoemission spectroscopy measurements were made with a VG Escalab 250 iXL ESCA instrument (VG Scientific), equipped with an aluminium Kα1,2 monochromatized radiation at 1,486.92 eV X-ray source. Photoelectrons were collected from a take-off angle of 90° relative to the sample surface. The measurement was made in a constant analyser energy mode with a 100 eV pass energy for survey spectra and 20 eV pass energy for high-resolution spectra. Charge referencing was done by setting the lower-binding-energy C 1s photo peak at 285.0 eV. The surface elemental composition was determined by using the standard Scofield photoemission cross-sections. The compositional analysis after 90 s of Ar-ion cleaning yielded an atomic ratio of Cr/N = 1.01(2), confirming the excellent control over the stoichiometry of the samples. A similar result of V/N = 1.02(3) was found for the samples of VN (see Supplementary Fig. S4).

X-ray powder patterns at different temperatures were collected in a diffractometer with a rotating anode with wavelength $\lambda = 1.5418$ Å (Cu Kα1) and a two-dimensional detector.

High-resolution X-ray diffraction under pressure (up to 20 GPa) was carried out at Station 9.5 HPT ($\lambda = 0.44397$ Å) of the Daresbury Synchrotron Radiation Source, UK (ref. 32), with diamond anvil cells from EasyLab. A 4:1 CH_3OH:C_2H_5OH mixture was used as the pressure medium. Ruby fluorescence was followed as an internal manometer before and after the measurement to check any possible relaxation of the pressure. Several runs with different samples were made under increasing and decreasing pressure, proving that the results are fully reversible and perfectly reproducible.

The temperature and pressure dependencies of the lattice parameters were obtained from the Rietveld fitting of the powder patterns at different temperatures with the program Rietica (http://www.rietica.org/index.htm). Standards of Si and LaB_6 were used as a reference to refine the instrumental parameters in the pressure and temperature equipment respectively (see Supplementary Figs S1 and S2).

Magnetic susceptibility under pressure up to 1 GPa was measured in a superconducting quantum interference device magnetometer in a commercial Be–Cu cell (from EasyLab). Daphne 7373 paraffin oil was used as the transmitting medium. The pressure dependence of the superconducting transition in Sn was used as an internal manometer.

Electrical resistivity was measured by the four-point method in a PPMS from Quantum Design. The measurements were made on sintered pellets previously pressed at ≈0.3 GPa in a tungsten carbide anvil.

Thermal conductivity was measured by the steady-state method in a home-made set-up (see Supplementary Fig. S6).

***Ab initio* calculations.** Calculations on the basis of the density functional theory were carried out with the WIEN2k software[33] and a full-potential, all-electron scheme on the basis of the APW + lo method[34]. The muffin-tin radii chosen were 1.99 a_0 for Cr and 1.76 a_0 for N, where a_0 is the Bohr radius. Local orbitals were added to improve the flexibility in dealing with semicore states (Cr 3*s* 3*p* and N 2*s*). All the calculations converged with respect to the parameters used, up to $R_{mt}K_{max} = 6$ and a k-mesh $12 \times 12 \times 12$ in the irreducible wedge of the Brillouin zone. The parameter $R_{mt}K_{max}$ controls the size of the plane-wave basis, and is defined as the product of the plane-wave cut-off and the smallest atomic-sphere radii (muffin-tin radii).

The value of the bulk modulus of CrN in both structures was calculated with the generalized gradient approximation as an exchange–correlation functional[35]. The paramagnetic phase was simulated by using the structural parameters in the paramagnetic regime and carrying out a non-magnetic calculation without considering the spin degrees of freedom of the system. Typical deviation within 5–10% with respect to experimental determinations is typically due to the quality of the fittings and the different numbers of points used.

The electronic structures of the low-pressure paramagnetic, cubic rock-salt structure and of the high-pressure AF orthorhombic structure were calculated by introducing strong correlations by means of the LDA + U method[36] to deal with the Cr d electrons. We used a value of $U = 4$ eV (effective U, $U - J$, where U is the on-site Coulomb repulsion and J the on-site Hund exchange coupling). The main conclusions of the paper are independent of the exact choice of U.

Received 12 February 2009; accepted 16 September 2009; published online 25 October 2009

References

1. Kaner, R. B., Gilman, J. J. & Tolbert, S. H. Designing superhard materials. *Science* **308,** 1268–1269 (2005).
2. Tong, W. P., Tao, N. R., Wang, Z. B., Lu, J. & Lu, K. Nitriding iron at lower temperatures. *Science* **299,** 686–688 (2003).
3. Esaka, R. *et al.* Comparison of surface oxidation of titanium nitride and chromium nitride films studied by X-ray absorption and photoelectron spectroscopy. *J. Vac. Sci. Technol. A* **15,** 2521–2528 (1997).
4. Gregoryanz, E. *et al.* Synthesis and characterization of a binary noble metal nitride. *Nature Mater.* **3,** 294–297 (2004).

5. Grossman, J. C. *et al.* Transition metals and their carbides and nitrides: Trends in electronic and structural properties. *Phys. Rev. B* **60,** 6343–6347 (1999).
6. McMillan, P. F. New materials from high-pressure experiments. *Nature Mater.* **1,** 19–25 (2002).
7. Subramanya Herle, P., Hegde, M. S., Vasathacharya, N. Y. & Philip, S. Synthesis of TiN, VN and CrN from ammonolysis of TiS_2, VS_2, and Cr_2S_3. *J. Solid State Chem.* **134,** 120–127 (1997).
8. Gall, D., Shin, C-S., Haasch, R. T., Petrov, I. & Greene, J.E. Band gap in epitaxial NaCl-structure CrN(001) layers. *J. Appl. Phys.* **91,** 5882–5886 (2002).
9. Corliss, L. M., Elliott, N. & Hastings, J. M. Antiferromagnetic structure of CrN. *Phys. Rev.* **117,** 929–935 (1960).
10. Browne, J. D., Liddell, P. R., Street, R. & Mills, T. An investigation of the antiferromagnetic transition of CrN. *Phys. Status Solidi A* **1,** 715–723 (1970).
11. Filippetti, A. & Hill, N. A. Magnetic stress as the driving force of structural distortions: the case of CrN. *Phys. Rev. Lett.* **85,** 5166–5169 (2000).
12. Angel, R. J. *High-Temperature and High-Pressure Crystal Chemistry* (Reviews in Mineralogy and Geochemistry, 41, Mineralogical Society of America, 2000).
13. Chen, H. Y., Tsai, C. J. & Lu, F. H. The Young's modulus of chromium nitride films. *Surf. Coat. Technol.* **184,** 69–73 (2004).
14. Aizawa, T., Kuwahara, H. & Tamura, M. Fabrication of CrN/Cr_2N bulk composites and their mechanical properties. *J. Am. Ceram. Soc.* **85,** 81–85 (2002).
15. Crowhurst, J. C. *et al.* Synthesis and characterization of the nitrides of platinum and iridium. *Science* **311,** 1275–1278 (2008).
16. Shebanova, O., Soignard, E. & McMillan, P. F. Compressibilities and phonon spectra of high-hardness transition metal-nitride materials. *High Press. Res.* **26,** 87–97 (2006).
17. Cumberland, R. W. *et al.* Osmium diboride, an ultraincompressible, hard material. *J. Am. Chem. Soc.* **127,** 7264–7265 (2005).
18. Yu, R., Zhan, Q. & De Jonghe, L. C. Crystal structures of and displacive transitions in OsN_2, IrN_2, RuN_2, and RhN_2. *Angew. Chem. Int. Ed. Engl.* **46,** 1136–1140 (2007).
19. Young, A. F. *et al.* Synthesis of novel transition metal nitrides IrN_2 and OsN_2. *Phys. Rev. Lett.* **96,** 155501–155504 (2006).
20. Chhowalla, M. & Unalan, H. E. Thin films of hard cubic Zr3N4 stabilized by stress. *Nature Mater.* **4,** 317–322 (2005).
21. Meng, Y. *et al.* The formation of sp^3 bonding in compressed BN. *Nature Mater.* **3,** 111–114 (2004).
22. Goodenough, J. B. *Magnetism and the Chemical Bond* (Wiley, 1963).
23. Goodenough, J. B. & Rivadulla, F. Bond-length fluctuations in transition-metal oxides. *Mod. Phys. Lett. B* **19,** 1057–1081 (2005).
24. Goodenough, J. B., Dutta, G. & Manthiram, A. Lattice instabilities near the critical V–V separation for localized versus itinerant electrons in $LiV_{1-y}M_yO_2$ (M = Cr or Ti)$Li_{1-x}VO_2$. *Phys. Rev. B* **43,** 10170–10178 (1991).
25. Radaelli, P. G. *et al.* Formation of isomorphic Ir^{3+} and Ir^{4+} octamers and spin dimerization in the spinel $CuIr_2S_4$. *Nature* **416,** 155–158 (2002).
26. Schmidt, M. *et al.* Spin singlet formation in $MgTi_2O_4$: Evidence of a helical dimerization pattern. *Phys. Rev. Lett.* **92,** 56402–56405 (2004).
27. Anderson, P. W. New approach to the theory of superexchange interactions. *Phys. Rev.* **115,** 2–13 (1959).
28. Harrison, W. A. *Electronic Structure and the Properties of Solids. The Physics of the Chemical Bond* (W. H. Freeman, 1980).
29. Bloch, D. The 10/3 law for the volume dependence of suprexchange. *J. Phys. Chem. Solids* **27,** 881–885 (1966).
30. Zhou, J.-S. & Goodenough, J. B. Pressure-induced transition from localized electron toward band antiferromagnetism in $LaMnO_3$. *Phys. Rev. Lett.* **89,** 87201–87204 (2002).
31. Haines, J. & Leger, J. M. Phase transitions in ruthenium dioxide up to 40 GPa: Mechanism for the rutile-to-fluorite phase transformation and a model for the high-pressure behaviour of stishovite SiO_2. *Phys. Rev. B* **48,** 13344–13350 (1993).
32. Lennie, A. R., Laundy, D., Roberts, M. A. & Bushnell-Wye, G. A novel facility using a Laue focusing monochromator for high-pressure diffraction at the SRS, Daresbury, UK. *J. Synchrotron. Radiat.* **14,** 433–438 (2007).
33. Schwarz, K. & Blaha, P. Solid state calculations using WIEN2k. *Comput. Mater. Sci.* **28,** 259–273 (2003).
34. Sjöstedt, E., Nördstrom, L. & Singh, D. J. An alternative way of linearizing the augmented plane-wave method. *Solid State Commun.* **114,** 15–20 (2000).
35. Perdew, J. P., Burke, K. & Ernzerhof, M. Generalized gradient approximation made simple. *Phys. Rev. Lett.* **77,** 3865–3868 (1996).
36. Lichtenstein, A. I., Asinimov, V. I. & Zaanen, J. Density-functional theory and strong interactions: Orbital ordering in Mott–Hubbard insulators. *Phys. Rev. B* **52,** R5467–R5470 (1995).

Acknowledgements

B. Dacuña from the X-ray service of USC (Spain) is acknowledged for his help during the thermal X-ray experiments, as are A. Lennie, S. Blanco-Canosa and M. Otero-Leal for their collaboration in the high-pressure X-ray experiments at Daresbury SRS. C. Serra from the University of Vigo, Spain, is acknowledged for the X-ray photoemission spectroscopy analysis. We acknowledge financial support from Xunta de Galicia (PXIB20919PR and O8PXIB236053PR) MEC of Spain (MAT2009-08165) and the Robert A. Welch Foundation of Houston, TX (Grant F-1066).

Author contributions

F.R. conceived the project, synthesized the samples, carried out the synchrotron and magnetic experiments, analysed the results and wrote the paper. M.B.-L. carried out and analysed the synchrotron X-ray data and participated in the discussion. C.X.Q. made electrical and thermal conductivity measurements, and collaborated in the synthesis. A.P., V.P. and D.B. carried out the *ab inito* calculations and participated in the discussions. M.A.L.-Q. and J.R. participated in the discussion. C.A.R. and H.S. measured the thermal expansion and Young modulus. J.-S.Z. carried out high-pressure X-ray experiments. J.B.G. participated in the discussion and wrote the paper.

Additional information

Supplementary information accompanies this paper on www.nature.com/naturematerials. Reprints and permissions information is available online at http://npg.nature.com/reprintsandpermissions. Correspondence and requests for materials should be addressed to F.R.